Pharm Res (2011) 28:1643–1652
DOI 10.1007/s11095-011-0399-4

RESEARCH PAPER

Influence of Particle Size on the Ultraviolet Spectrum of Particulate-Containing Solutions: Implications for *In-Situ* Concentration Monitoring Using UV/Vis Fiber-Optic Probes

Bernard Van Eerdenbrugh • David E. Alonzo • Lynne S. Taylor

Received: 3 December 2010 / Accepted: 9 February 2011 / Published online: 4 March 2011

ABSTRACT

Purpose To critically evaluate the effect of submicron and micron-sized organic particulates on the ultraviolet (UV) absorption spectra of aqueous systems and assess the applicability of UV/Vis fiber-optic probes for *in-situ* concentration monitoring in the presence of particles of different sizes.

Methods UV absorbance spectra were obtained for aqueous felodipine suspensions containing a range of particle sizes (300 nm–400 μm) and suspension concentrations and for methanolic solutions of different concentrations and amorphous films of different thicknesses. Select suspensions were further characterized using nuclear magnetic resonance (NMR) experiments. Mie theory was used to provide insight into the role of particle size on scattering and absorption of UV radiation.

Results Large increases in absorbance as a function of total suspension concentration were observed for nanosuspensions but not for the other particle sizes evaluated. NMR measurements of solution concentration indicated that the observed increases in UV absorbance values for these systems were not caused by increases in the concentration of dissolved molecules, implying that nanoparticles of felodipine might absorb UV light. Mie theory-based calculations enabled reconstruction of the experimental observations and supported this hypothesis.

Conclusions For solutions containing small (submicron) felodipine particles, UV spectra were influenced by absorption of the particles and contributions from absorption of dissolved molecules and scattering of the particles. Caution should be applied when using *in situ* UV/VIS-probes to monitor the amount of dissolved material during dissolution, in particular when small particles are present (e.g. dissolution of nanoparticulate formulations) or generated (e.g. precipitation of supersaturated solutions) in the dissolution medium.

KEY WORDS concentration measurement · fiber-optic probes · Mie theory · nanoparticles

B. Van Eerdenbrugh · D. E. Alonzo · L. S. Taylor (✉)
Department of Industrial and Physical Pharmacy, College of Pharmacy
Purdue University
575 Stadium Mall Drive
West Lafayette, Indiana 47907, USA
e-mail: lstaylor@purdue.edu

B. Van Eerdenbrugh
Laboratory for Pharmacotechnology and Biopharmacy, K.U. Leuven
Gasthuisberg O&N2, Herestraat 49, box 921, 3000 Leuven, Belgium

INTRODUCTION

Determination of solution concentration, particularly within the framework of dissolution testing, is an important technique in the evaluation of drug products, both during formulation development and as a quality control tool. Traditionally, quantification of the dissolved drug concentration in the dissolution medium as a function of time is performed by removing samples from the dissolution vessel followed by filtration and subsequent ultraviolet (UV) or high performance liquid chromatography combined with UV analysis (HPLC-UV). An increasingly important alternative to these traditional techniques is the *in situ* measurement of dissolution profiles using fiber-optic UV/Vis probes. These probes are also finding widespread use for concentration determination in applications such as the miniaturized analysis of (intrinsic) dissolution rates using a rotating disk (1,2) or powder (3), estimations of particle sizes based on dissolution rate data (4), and determination of precipitation behavior in artificial stomach-duodenum models (5).

The use of *in situ* fiber-optic probes for concentration monitoring during dissolution testing was first explored in the late eighties, using a variable wavelength spectrophotometer and felodipine tablets as the model system (6). Subsequent methodology advancements include integration of diode array spectrophotometers (7), development of instrumentation enabling the simultaneous evaluation of multiple dissolution vessels (e.g. through the use of multiple probes in combination with a transport accessory that allows the light beam to be switched between the different probes (8) or through the use of a charge-coupled device (CCD) (9,10)) and the integration of robotics for the movement of a single probe between different dissolution vessels (11–13). Other studies detail the use of different probe designs (e.g. transmission *versus* transflectance probes, or probes with variable path length) (14–23) as well as the validation efforts necessary to implement the technology in pharmaceutical settings (24–26). A number of clear advantages can be associated with the use of *in situ* fiber-optics. The first advantage is the elimination of sampling; hence, sampling consumables (filters, solvents etc.) are eliminated, as is the subsequent off-line analysis. Second, through the use of fiber-optics, real-time and frequent sampling is possible, resulting in more extensive datasets that allow for a more thorough characterization of concentration-time profiles and hence the dissolution process.

Accompanying the aforementioned advantages are several analytical challenges which are often circumvented with traditional sampling techniques. For example, when using a combination of filtration and HPLC separation for quantification, interference from absorption of dissolved excipients typically can be prevented. This is not always the case when using fiber-optic probes (27); however, successful examples exist where solution drug concentrations were accurately measured in the presence of interfering dissolved species through the use of multivariate chemometric methods (28) or three-wavelength K-ratio spectrophotometry (29). Two other important sources of interference that can impact the analysis when filtration is not performed prior to measurement are insoluble excipient particles as well as particles arising from the drug itself. In current literature reports (1–29), scattering is reported as being the sole interfering effect of insoluble particles during *in situ* fiber-optic dissolution experiments. The influence of scattering on the observed spectra is an apparent increase in absorbance. This increase can be constant over a wide wavelength range or can increase with decreasing wavelengths, resulting in baseline distortions. In the former case, a relatively simple baseline offset correction can be applied, e.g. using a single compensation wavelength at a wavelength where the observed absorbance is solely due to scattering. The latter case, where scattering increases with decreasing wavelength, is known as Tyndall scattering, and second derivative algorithms can often be successfully applied to correct for this baseline phenomenon. The aforementioned approaches have been frequently applied to correct for scattering effects, yielding dissolution curves in good agreement with those obtained from traditional sampling techniques.

However, in addition to scattering, it is well known from particle physics that absorption can contribute to the attenuation or extinction of electromagnetic (EM) radiation incident on a particle (30,31). Hence, the underlying assumption made in the studies referenced above, namely that extinction of EM radiation by particles is exclusively the result of scattering and that the only absorption occurring is due to individual drug or excipient molecules present in the solution phase, is not necessarily valid from a theoretical perspective. In reality, molecules that absorb light do not necessarily need to be in solution to do so. The absorption of light by particulates is, however, size dependent and is of greatest relevance for smaller particles. While the absorption properties of, e.g. metal nanoparticles, have been described extensively (32–34), literature on organic nanoparticulate systems is sparse (e.g. (35)) and has, to the best of our knowledge, never been related to the applicability of UV/Vis fiber-optic probes for solution concentration determination. Regarding absorption and scattering of light, it is of relevance to briefly mention Mie theory, a well-known theoretical framework that can be used to simulate the interaction of EM radiation with a (spherical) particle (30,31). This theory enables calculation of the relative amounts of light scattered and absorbed by a spherical particle of arbitrary size, its sum being termed extinction. The outcome depends on several parameters, including the real refractive indices of both the particle and the surrounding medium, the wavelength of the incident light, the particle size and the absorptivity of the particle, expressed through its imaginary refractive index. As a general rule, absorption dominates extinction for a given particle with a sufficiently small diameter. As particle size increases, scattering becomes increasingly important. The above considerations suggest that current practice where corrections are only made for the scattering effects of undissolved particles may not be adequate for the accurate determination of the dissolved drug concentration; while scattering corrections may be applicable for systems where the suspended particles are sufficiently large, in cases where smaller particles are present in the dissolution medium the validity of this approach needs to be reevaluated. Potential scenarios resulting in smaller particles include cases where the drug has been formulated as a nanosuspension (36–38), small particles are formed upon dissolution of larger particles or precipitation occurs from either a supersaturating drug delivery system (39) or because of a pH-induced change in solubility. It should be stressed that the current

trend of new potential drug candidates having lower aqueous solubility (40) often necessitates the formulation of drugs as either smaller particles or as a supersaturating drug delivery system.

Given the increasing use of *in situ* fiber-optic probes coupled with UV spectroscopy for the characterization of pharmaceutical systems, it is clearly of importance to understand the impact of particulates on the resultant spectra. The purpose of this study was therefore to characterize the impact of particle size and concentration on absorption and scattering of light in the UV/Vis region of the EM spectrum. Felodipine was selected as a model drug. Fiber-optic probes coupled to a UV/Vis spectrometer were employed to generate spectra of felodipine suspensions of various size ranges (300 nm–400 μm) as a function of total suspension concentration. Mie theory calculations were undertaken to provide insight into the underlying phenomenon taking place. The potential impact of these findings with respect to *in situ* fiber-optic UV/Vis probes for dissolution monitoring is discussed.

MATERIALS AND METHODS

Materials

Felodipine was a gift from AstraZeneca (Södertälje, Sweden). Polyvinylpyrrolidone (PVP, Kollidon® 30) was kindly provided by BASF Corporation (Mt. Olive, NJ). Dichloromethane (ChromAR®) and methanol (anhydrous, ChromAR®) were purchased from Mallinckrodt Baker, Inc., Phillipsburg, NJ, USA. Ethyl alcohol (200 proof) was purchased from Pharmco Products, Inc., Brookfield, CT, USA and Aaper, Shelbyville, KY, USA.

Sample Preparation

Felodipine nanosuspensions were prepared using media milling. PVP (100%, relative to the drug weight) was selected for nanosuspension stabilization based on an initial screening using different stabilizing agents at different concentrations (data not shown). For the purpose of this study, a nanosuspension is defined as a suspension of submicron drug particles (36–38). Suspensions of 0.5 g of felodipine were dispersed in the aqueous stabilizer solution (0.5 g PVP in 5 ml water) in 20 ml scintillation vials (Research Products International Corp., Mt. Prospect, IL); 8 batches were prepared in total. Subsequently, 5 g of zirconium oxide beads (ø 0.5 mm, YTZ® grinding media, Tosoh Corporation, Tokyo, Japan) were added as a milling agent together with a magnetic stirring bar (starburst, diameter 3/4″). The vials were placed on a stirring plate (Telesystem HP 60, Variomag® U.S.A., Daytona Beach, FL), and stirring was performed at 100 rpm. Particle size of the batches was monitored using dynamic light scattering (DLS, see below). Milling was halted when DLS indicated that a mean particle size of around 300 nm had been obtained. Different milling times were applied for the different batches, as milling efficiency tended to vary from batch to batch. Subsequently, the 8 batches were combined and transferred into a 100 ml glass cylinder. To further separate off larger particles and agglomerates, the cylinder was allowed to stand overnight, followed by isolation of the supernatant nanosuspension. Herein, *total suspension concentration* will be used to describe the concentration of both dissolved and undissolved felodipine. The terms *dissolved felodipine concentration, solubility and solution concentration* denote the dissolved material only. The total felodipine concentration in the nanosuspension was determined by high pressure liquid chromatography (HPLC). Aqueous dilutions of this nanosuspension were made in order to obtain experimental samples at select concentrations as indicated in the Results and Discussion section. The final PVP concentration of these samples was kept constant at 1 mg/ml. Jetmilling was performed using a home-built apparatus. After jetmilling, the collected powder was sieved through a 53 μm mesh. Manual grinding of bulk felodipine powder was performed using a mortar and pestle. Subsequently, 300–500, 106–250 and 53–106 μm size fractions were isolated by sieving ("Sieved Fraction 1, 2 and 3"). Suspensions of the jetmilled and ground powders were prepared by adding the solids to an aqueous PVP solution (100% PVP, relative to the drug weight), followed by sonication for 10 min, and then were allowed to stand for at least 60 min. Aqueous dilutions of the suspensions were prepared for further measurements, keeping the final PVP concentration constant at 1 mg/ml. All experiments were performed at room temperature. Further physicochemical characterization of the obtained powders and the freeze-dried nanosuspension using differential scanning calorimetry (DSC), X-ray powder diffraction (XRPD), Raman and mid-infrared spectroscopy confirmed the presence of crystalline felodipine and pointed to the absence of amorphous felodipine (data not shown).

Dynamic Light Scattering (DLS)

Dynamic light scattering experiments were performed on the nanosuspensions for the determination of particle sizes. A Malvern Zetasizer ZS® (Worchestershire,UK) series instrument, equipped with a 173° backscattering detector, was used for these measurements. The temperature was set at 25°C, and the attenuation and measurement settings were optimized automatically by the resident software. Disposable cuvettes (VWR International, West Chester, PA USA) were used. Measurements were performed in duplicate.

Particle Size Evaluation Using Laser Diffraction (LD)

LD was used to characterize the particle size distributions of the samples, using a Mastersizer 2000 equipped with a Hydro MU sample dispersion unit (Malvern Instruments Limited, Worcestershire, UK). Except for the nanosuspension, which was used as such, the following procedure was applied for sample preparation: 1 g of felodipine powder was suspended in 5 ml of a 100 mg/ml PVP aqueous solution in 20 ml scintillation vials. Subsequently, the suspensions were stirred vigorously with a vortex mixer, followed by ultrasonic treatment of the samples for 15 min using an ultrasonic bath. Given the low aqueous solubility of felodipine (about 0.81 μg/ml at room temperature (41)), water was selected as the dispersing medium. Analysis of the resultant diffraction patterns was performed using the Mie model (30,31). Each measurement was performed in triplicate. From the resulting volume distributions of both batches, the average 10, 50 and 90% volume percentile values ($d_{(v,0.1)}$, $d_{(v,0.5)}$ and $d_{(v,0.9)}$) and span of the distribution (span = $(d_{(v,0.9)} - d_{(v,0.1)})/d_{(v,0.5)}$) were determined, as well as their standard deviations.

Nuclear Magnetic Resonance Spectroscopy (NMR)

NMR spectroscopy was employed to evaluate the effect of particle size on solubility. Therefore, the solubility of the nanoparticles was compared to that of coarse particles of felodipine. An excess of solid was added to 10 ml of a mixture of ethanol/water (25/75 (v/v)) in 20 ml scintillation vials (Research Products International Corp., Mt. Prospect, IL). The latter solvent system was used to increase felodipine solubility and, hence, the signal-to-noise ratio of the measurements. Subsequently, the suspensions were stirred for 24 h to allow for equilibration. A 1 ml aliquot of the suspension was transferred into an NMR sample tube (type 528-PP-7, Wilmad LabGlass, Vineland, NJ). 1D proton NMR spectra were acquired at 25°C using a Bruker AVANCE DRX500 spectrometer equipped with an inverse proton cryoprobe and single axis (z) gradient. The total inter-scan delay was 5 s, sweep width was 16 ppm, and a total of 16 K complex data points were acquired. Solvent water and ethanol were suppressed by a WET sequence that selects multiple resonances with minimal impact to the aromatic signals of felodipine. For felodipine solubility determination, the aromatic peaks were integrated after the free induction decay (FID) was processed with a mild window function (0.3 Hz exponential multiplication), Fourier transformation, manual phasing and baseline corrections. All experiments were performed in triplicate, with each spectrum acquired with 256 scans. The averages and standard deviations were calculated. Solubilities of the nanoparticles were expressed relative to that of the coarse powder reference.

UV/Vis Spectral Analysis Using Fiber-Optic Probes

UV/Vis spectra were obtained using a 6-channel fiber-optic system (Ocean Optics, Dunedin, FL, USA), consisting of a DH-2000-BAL light source, six 1 cm pathlength transflectance dip probes (T300-RT-UV-VIS) and a Jaz spectrometer module. Wavelength scans (<1 nm resolution) were performed on samples at 25°C from 200 nm to 700 nm. Calibration solutions (0.5–20 μg/ml) were prepared in methanol. A Savitzky-Golay smoothing function with a second-order polynomial (40 points of window) was applied to the spectra, using OriginPro 8 SR1 (v8.0773, OriginLab Corporation, Northampton, MA) (42). Spectral peaks and absorption intensities were not altered by this treatment. For further quantification purposes, second derivatives of the spectra (range 270–440 nm) were taken for the calibration and sample data in order to mitigate particle scattering effects.

UV/Vis Spectral Analysis Using Offline Equipment

For these experiments, a Cary 300 Bio instrument with WinUV software (Varian Inc., Palo Alto, CA) was used in double beam mode. For the measurement of the spectrum of a 0.81 μg/ml felodipine solution in methanol, quartz cuvettes were used (10 mm pathlength, Starna Cells, Inc., Atascadero, CA, USA). In order to estimate the imaginary refractive index (absorbance) of felodipine (see below), amorphous films of various thicknesses were prepared by spin-coating solutions of felodipine in dichloromethane on quartz cover slips (19×19 mm, Chemglass Life Sciences, Vineland, NJ). Amorphous films were preferred here above crystalline samples, as spectral contributions due to scattering were found to be negligible for the former. The spin-coating procedure and estimation of the average film thickness (based on weight gain of the cover slips) has been previously described in more detail (43). As such, 4 films were prepared, covering an average thickness range from 0.52 to 1.58 μm. Three separate measurements were performed on each film from which the average absorbance at 361 nm (peak maximum) was determined, together with the corresponding standard deviation.

Mie Model Simulations

Simulations were performed using MiePlot v4.2.03 (http://www.philiplaven.com/mieplot.htm), a Visual Basic interface to the BHMIE code, originally developed by Bohren and Huffman (31). Simulations were performed using a real refractive index of 1.57 (44) for felodipine and 1.33 for water. The imaginary part of the refractive index was estimated from spectral data obtained on amorphous felodipine films (see above), assuming reflection to be

negligible at the interfaces of the films, using the following equations (31):

$$\alpha = \frac{4\pi k}{\lambda} \tag{1}$$

$$\alpha h = \ln \frac{I_0}{I} \tag{2}$$

Where α is the absorption coefficient, λ the wavelength, k is the imaginary part of the refractive index, h the thickness of the film and I_0 and I the incident and transmitted intensities, respectively. Upon calculation of $\ln(I_0/I)$, derived from the absorbance measurements for the different films with average film thickness h, α was estimated to be $4.0 \pm 0.4\ \mu m^{-1}$ at 361 nm. From this, a k value of 0.116 ± 0.013 was obtained. Based on the relationships shown by Eqs. 1 and 2 and using the spectrum of an amorphous felodipine film, additional values of k were determined at different wavelengths between 275 and 500 nm, at 5 nm intervals. The latter were used to calculate the extinction cross-sections (C_{ext}, the sum of the scattering and absorbance cross sections) using MiePlot v4.2.03 as a function of wavelength for spherical particles of different sizes with the absorbance properties of felodipine. Similar simulations were performed for nonabsorbing spherical particles, using a k value of zero at all wavelengths. To allow comparison with absorbance measurements, the obtained extinction cross sections were further converted into $-\log(I/I_0)$ values, since absorbance is defined as

$$A_{\lambda,h} = -\log \frac{I}{I_0} \tag{3}$$

with $A_{\lambda,h}$ the absorbance at a specified wavelength, λ, I the intensity of light at that wavelength that has passed through a sample of thickness, h, and, I_0, the intensity of the incident light. Transformation of the extinction data can be performed by considering Bohren and Huffman (Chapter 11, Section 11.1, with some modification of symbols) (31): *"If multiple scattering is negligible the irradiance of a beam of light is exponentially attenuated from I_0 to I in traversing a distance h through a particulate medium:*

$$\frac{I}{I_0} = \exp(-\alpha_{ext} h) \tag{4}$$

Extinction is the result of both absorption and scattering (α_{ext} is the attenuation coefficient; note that this is not the same as the absorption coefficient, α, defined above).

$$\alpha_{ext} = N(C_{abs} + C_{sca}) \tag{5}$$

N is the number of particles per unit of volume, C_{abs} and C_{sca} are the absorption and scattering cross sections, respectively."

Based on this, Eq. 4 can be rewritten as

$$\ln \frac{I}{I_0} = -\alpha_{ext} h \tag{6}$$

which can be further expressed as

$$-\log \frac{I}{I_0} = \frac{a_{ext} h}{\ln(10)} \tag{7}$$

The extinction cross-section, C_{ext} equals (31)

$$C_{ext} = C_{abs} + C_{sca} \tag{8}$$

Hence, upon introduction of V_{part}, the volume of a particle, and with $C_{ext,V}$ ($=C_{ext}/V_{part}$, the extinction cross-section per unit of volume), Eq. 5 can be rewritten as

$$\alpha_{ext} = N V_{part} C_{ext,V} \tag{9}$$

Thus, Eq. 7 becomes

$$-\log \frac{I}{I_0} = \frac{N V_{part} C_{ext,V} h}{\ln(10)} = K C_{ext,V} \tag{10}$$

the constant K being defined as

$$K = \frac{N V_{part} h}{\ln(10)} = \frac{\phi_{part} h}{\ln(10)} \tag{11}$$

with ϕ_{part} ($= N V_{part}$) the volume fraction of the particles.

For these calculations, a pathlength of 1 cm, a particle concentration of 50 μg/ml and the density of crystalline felodipine of 1.451, derived from the crystal structure (DONTIJ) (45), were used.

RESULTS AND DISCUSSION

UV/Vis spectra of felodipine nanosuspensions (Z-average particle diameter = 300 ± 3 nm, polydispersity index = 0.141 ± 0.006, by DLS) as a function of total nanosuspension concentration are depicted in Fig. 1. Clearly, with increasing total nanosuspension concentration, both the scattering contribution as well as that due to absorption increase. The observed scattering, which shows the Tyndall effect, is a well-described phenomenon that can be corrected using a second derivative approach. However, the increase in absorption suggests, based on conventional interpretation, that the concentration of dissolved felodipine increases with increasing total nanosuspension concentration. Upon comparison of these spectra with the spectrum from a methanolic solution of felodipine equal in concentration to its aqueous solubility (0.81 μg/ml (41)), the absorbancies of the nanosuspensions greatly exceed the latter. At first glance, these results might be interpreted as the nanoparticulate systems giving rise to a higher solubility due to the higher curvature of the nanoparticles. However,

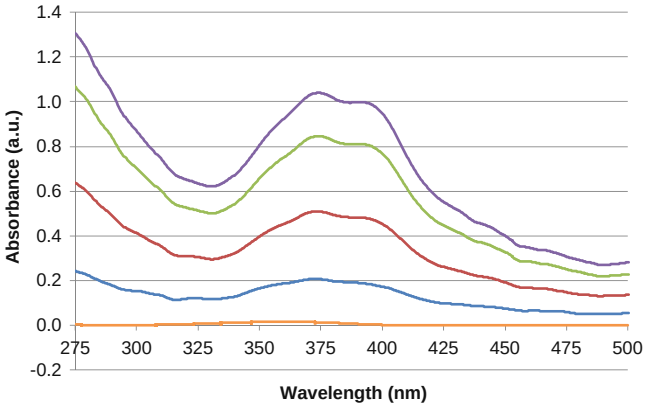

Fig. 1 UV-Vis spectra, measured with fiber-optic probes: 0.81 μg/ml felodipine solution in methanol (), felodipine nanosuspensions of 10(), 25(), 40() and 50() μg/ml total felodipine concentration.

both the Ostwald-Freundlich equation (46) and an experimental study suggest that the actual relative solubility increases associated with crystalline drug nanoparticles of this size range are generally moderate (100–115% of equilibrium solubility) (47). Physicochemical characterization of the freeze-dried nanosuspension using DSC, XRPD, Raman and mid-infrared spectroscopy pointed to the absence of amorphous felodipine (data not shown), eliminating solubility enhancement due to a high energy solid form as the cause of the enhanced absorption. Additionally, it should be noted that even if a (small) fraction of amorphous felodipine were present in the nanosuspensions, it would be expected to spontaneously revert to the crystalline form through surface crystallization of the hydrated matrix (48) or by dissolution combined with growth of crystalline regions (49). The impact of dissolved PVP on the equilibrium solubility of felodipine was also investigated and found to be negligible. Significant increases in equilibrium solubility were not observed until the PVP solution concentration was above 5 mg/ml, more than 5 times the concentration used in this study (data not shown). However, to further verify that the increases in absorption intensity were not due to an increased concentration of dissolved molecules, NMR spectroscopy was used to determine solubilities in an ethanol/water mixture (25/75 (v/v)). The latter mixture was used to increase solubility relative to that in pure water, resulting in better signal-to-noise ratios for the NMR experiments. The obtained solubility of the nanosuspension was 89±10% of that of the coarse suspension. This result independently confirms that solubility increases are not responsible for the large increases observed in the absorbance spectra. Consequently, the contribution of the particulate matter to the increased intensity in the absorbance band of felodipine needs to be further explored.

Fig. 2 shows the UV/Vis spectra of suspensions containing jetmilled felodipine crystals ($d_{(v,0.1)}$=3.12±0.28 μm, $d_{(v,0.5)}$=10.19±0.64 μm, $d_{(v,0.9)}$=26.52±3.11 μm and span=2.29±0.13) as a function of total suspension concentration. Upon comparison of the data with that obtained from the nanosuspension (Fig. 1), a number of distinct differences can be noted. First, it is clear that scattering contributions to the spectra are greatly reduced and relatively constant over the depicted spectral range (i.e. the Tyndall effect is less pronounced). Second, and more important with respect to this study, the maximum intensity of the felodipine absorption peak that would be obtained after subtraction of the scattering component appears to be relatively constant and similar to that obtained for a methanolic solution with a felodipine concentration corresponding to its aqueous solubility (0.81 μg/ml (41)), irrespective of the total felodipine concentration of the suspension. Similar spectral observations were obtained for the other particle sizes investigated, but, for the sake of brevity, the spectral data are not shown. Instead, an exercise has been performed to quantitatively compare the predicted solution concentration derived from spectra obtained from suspensions containing different sized particles in order to assess to what extent the presence of particulates interferes with the determination of solution concentration values. As can be seen from Table I, $d_{(v,0.5)}$ values of the different suspensions cover three orders of magnitude. Apparent solution concentrations of the suspensions were estimated from the UV spectra obtained from samples containing different total suspension concentrations after taking a second derivative. The resultant analysis (Fig. 3) shows that, except for the nanosuspension, the estimated solution concentration remains relatively flat as a function of total felodipine concentration, although there is a slight trend of higher predicted dissolved concentrations with increasing

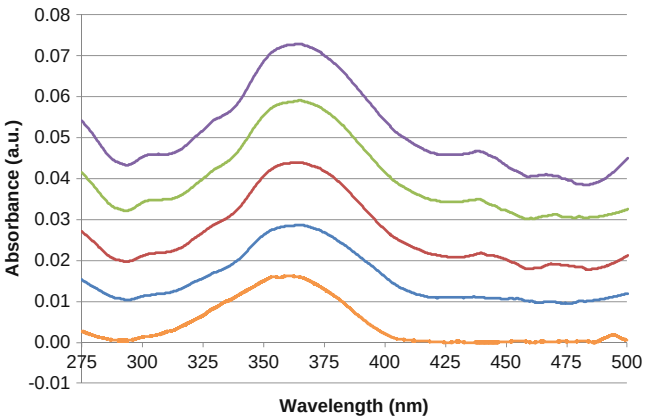

Fig. 2 UV-Vis spectra, measured with fiber-optic probes. 0.81 μg/ml felodipine solution in methanol (), suspensions of jetmilled felodipine of 10(), 25(), 40 () and 50() μg/ml total felodipine concentration.

Table I Particle size Data (LD, with Standard Deviations) of the Different Suspensions Evaluated ($n = 3$)

Suspension ID	$d_{(v,0.1)}$ (μm)	$d_{(v,0.5)}$ (μm)	$d_{(v,0.9)}$ (μm)	Span
Nanosuspension	0.15 ± 0.00	0.38 ± 0.04	1.90 ± 0.07	4.61 ± 0.24
Jetmilled	3.12 ± 0.28	10.19 ± 0.64	26.52 ± 3.11	2.29 ± 0.13
Sieved Fraction 1	6.71 ± 0.23	38.39 ± 0.46	96.88 ± 0.22	2.35 ± 0.03
Sieved Fraction 2	8.98 ± 0.47	105.03 ± 3.12	239.86 ± 1.47	2.20 ± 0.06
Sieved Fraction 3	226.09 ± 1.27	380.21 ± 0.08	601.34 ± 0.40	0.99 ± 0.00

suspension concentrations. The solution concentrations predicted for the suspensions should represent the equilibrium solubility of felodipine. The fact that the solution concentrations estimated at higher particle densities (up to 2.10 μg/ml) are large relative to the reported solubility of felodipine (about 0.81 μg/ml at room temperature (41)) most likely originates from the low absolute magnitude of the absorbance peak for a saturated solution of felodipine (with a corresponding peak maximum of only 0.034 a.u.), arising from its low aqueous solubility. Hence, small absolute errors resulting from the quantification procedure would appear as large relative errors. As these deviations are relatively small compared to those observed for the felodipine nanosuspension, the root cause of these deviations will not be further explored here. Indeed, the impact of the felodipine nanoparticles on the UV/Vis spectra as well as on the solution concentration estimates, even following a second derivative correction, is dramatic. A steep increase in the predicted dissolved concentration can be noted with particle concentration. As this cannot be attributed to actual solubility increases, this observation strongly suggests that submicron felodipine particles absorb light in a manner similar to free felodipine molecules in solution. As a result, concentration measurements in the presence of these submicron particles, with or without the corrective measures discussed above, yield much higher apparent solution concentrations than are actually present. Linear regression of the data points shown in Fig. 3 for the nanosuspensions yields a slope of 0.14 ($R^2 = 0.995$). In other words, for each increase in particle concentration of 10 μg/ml, an apparent increase in solution concentration of 1.4 μg/ml results. It is relevant to note at this juncture that, from a theoretical perspective, based on Mie theory, absorption effects of smaller particles would be expected to be higher, which is discussed in greater detail below. From an application viewpoint, this type of particulate interference clearly cannot be ignored and jeopardizes the accuracy of solution concentration estimates that are based on UV spectra obtained in the presence of these absorbing submicron particles.

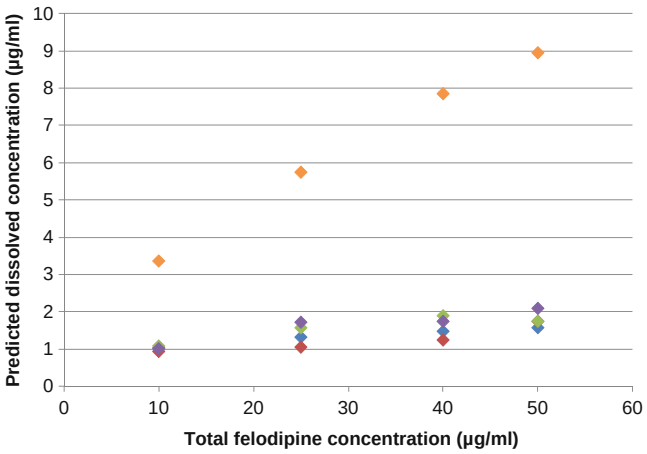

Fig. 3 Predicted solution concentration as a function of total felodipine suspension concentration: nanosuspension (◆), jetmilled (◆), sieved fraction 1 (◆), 2 (◆) and 3 (◆).

The experimental observations described above demonstrate that, for nanoparticles, there is indeed significant absorption in the region of the felodipine absorption band. It is therefore of interest to interpret these observations within the theoretical framework provided by Mie theory (30,31). Figure 4a–c depict the theoretically calculated extinction plots ($-\log(I/I_0)$) as a function of incident wavelength for spheres of different size either having the absorption properties of felodipine or being nonabsorbing. These were based on Mie calculations of extinction cross-sections that were further transformed into $-\log(I/I_0)$ units, assuming multiple scattering effects to be negligible, and a suspension concentration of felodipine particles of 50 μg/ml (see the Materials and Methods Section for further details), to allow for comparison with actual measurements of the 300 nm nanosuspension at that total felodipine concentration (included in Fig. 4a). Figure 4a shows results for particles with sizes from 30 to 300 nm. For nonabsorbing spheres, the extinction is solely due to scattering. With increasing size, $-\log(I/I_0)$ increases dramatically and shows an increasing trend with decreasing wavelength, in line with the Tyndall effect. Results obtained for particles having the absorbing properties of felodipine clearly demonstrate an additional increase in extinction in the region where felodipine absorbs. Both in absolute and relative terms (compared to the $-\log(I/I_0)$ values of nonabsorbing spheres), this increase in absorption becomes smaller with increasing size. Similar to dissolved molecules, it is the dominant form of extinction for 30 nm particles. For the 300 nm particles, scattering is predicted to be the dominant mechanism of extinction; however, the absorp-

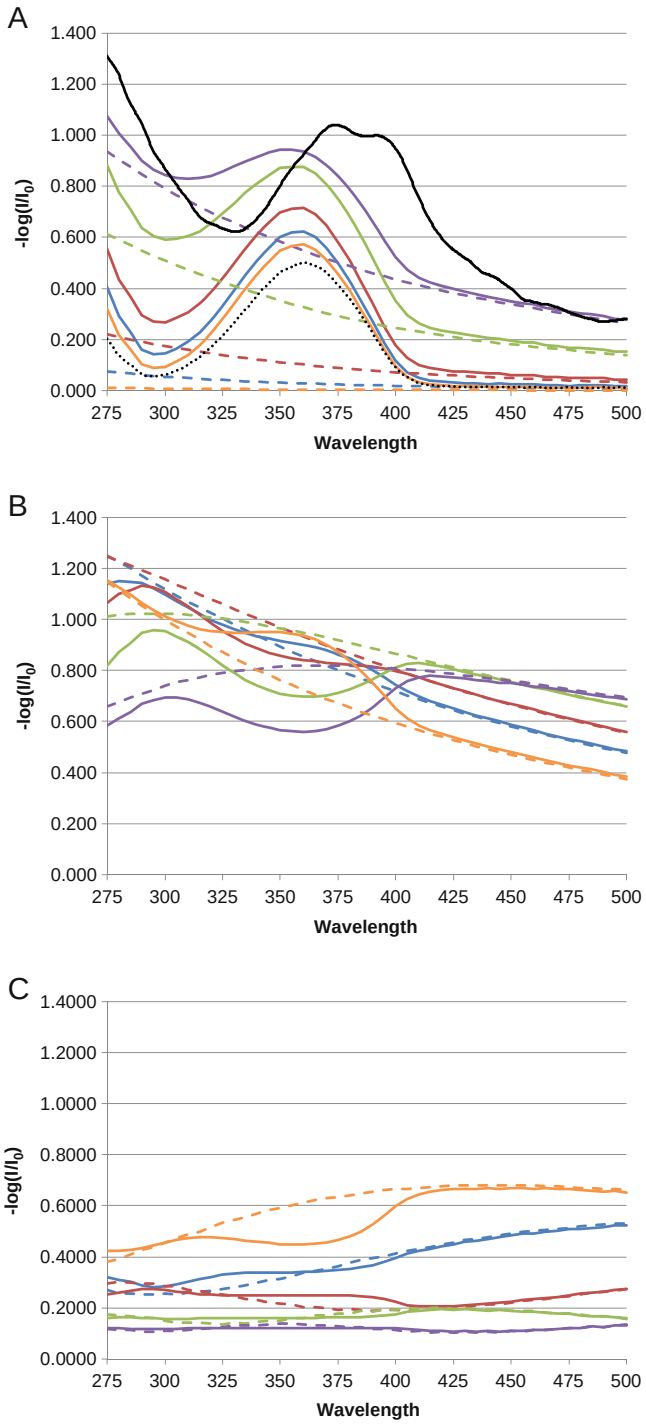

Fig. 4 Theoretically generated extinction [$-\log(I/I_0)$] plots as a function of the wavelength of the incident light for 50 μg/ml suspensions of nonabsorbing (dashed lines, $k = 0$ at all wavelengths) spheres, spheres with absorbance properties similar to those of felodipine (solid lines) for particles having different sizes, and experimentally measured spectrum of a 50 μg/ml felodipine nanosuspensions: (**A**) 30 (—), 60 (—), 100 (—), 200 (—), 300 (—) nm particles, the nanosuspension (—) and an amorphous film (•••••, maximum scaled to an absorbance of 0.5 a.u.); (**B**) 400 (—), 500 (—), 600 (—), 800 (—) and 1000 (—) nm particles; (**C**) 1200 (—), 1500 (—), 2000 (—), 3000 (—) and 4000 (—) nm particles. The sizes given represent the diameter of the particles.

tion contribution is certainly still significant for this particle size. The good agreement between the $-\log(I/I_0)$ graph calculated for the 300 nm particles and the experimentally measured spectrum for the 300 nm nanosuspension, in terms of the magnitude of the extinction, should be noted. Differences in the local environment of the felodipine molecules in the crystalline nanoparticles *versus* those in the amorphous state most likely underlie the differences seen in the shape of the felodipine absorbance peak between the curves, as absorbance measurements on amorphous films were used to calculate the imaginary refractive indexes used in the Mie calculations. The similarity seen in the shape of the absorbance peaks in the Mie predictions of Fig. 4a with that of an amorphous felodipine film (Fig. 4a, normalized to a maximum absorbance of 0.5 a.u.) further supports this reasoning. The above simulations clearly illustrate the underlying cause for the observed increases in absorbance seen for the nanosuspensions, namely that absorbance by the particles cannot be neglected. For particle sizes ranging from 400 to 1000 nm (Fig. 4b), a further decrease in the contribution of absorbance to the extinction of the spheres can initially be noted (400 and 500 nm particles). Subsequently (600, 800 and 1000 nm particles), the $-\log(I/I_0)$ patterns as a function of size become more complex. Nonabsorbing spheres lose their typical Tyndall pattern as $-\log(I/I_0)$ tends to rise more moderately (600 nm), level off (800 nm) or even decrease (1000 nm) at the lower wavelengths. This may even make the quantification routines applied problematic in the presence of nonabsorbing (excipient) particulates of such sizes. For the absorbing spheres, a decrease in $-\log(I/I_0)$ in the region of felodipine absorption is now observed. Although less straightforward to directly link the observed patterns to the absorbance of felodipine films now (spectrum included in Fig. 4a), their complexity suggests a potential source of error which may not be easily identified when estimating the concentration of a suspension within this particle size range. Similar observations can be made for the particles having sizes above 1000 nm (Fig. 4c, 1200–4000 nm), where it is interesting to note that above 2000 nm the extinction appears to take on the shape of a horizontal baseline, as often assumed in literature. However, three important trends can be seen here. First, $-\log(I/I_0)$ clearly tends to decrease with increasing particle size (note that the scale of the Y-axes in Fig. 4a–c are identical), as does its wavelength dependency. In addition, differences between nonabsorbing and absorbing spheres become smaller. From this modeling of organic particulate spectra, it is apparent that upwards of a certain particle size, offsetting baselines or taking a second derivative might be appropriate spectral correction routines to improve for the quantification of solution concentration.

It should be noted that the Mie theory calculations presented above rely on a number of simplifications and

assumptions, e.g. homogeneous monodisperse spheres were considered, the imaginary portion of the refractive index was estimated using amorphous films, the real part of the refractive index was an estimate and considered wavelength-independent and the Kramers-Kronig relationship between the real and imaginary refractive index was not taken into account. That being said, the insights provided by the simulations are consistent with the experimental observations in this study, supporting the conclusion that the presence of small particles (certainly nanoparticles) may impact the results of concentration measurements obtained using UV/Vis fiber-optic systems. Furthermore, in contrast with interferences of dissolved excipients and large particulates, spectral influences of small particulates seem to be much more complex, making deconvolution of contributions of dissolved drug and particulate material extremely challenging compared to correcting for dissolved excipient or large particle interferences.

CONCLUSIONS

The above results clearly demonstrate that there are limitations to the applicability of *in situ* UV/Vis fiber-optic probes for the measurement of solution concentrations in the presence of particulate matter. Hence, in any scenario where small (submicron) absorbing particles are present in the medium being analyzed, caution should be exerted when using UV/Vis fiber-optics for quantification of dissolved concentrations. Aside from where drugs are intentionally formulated as such (e.g. nanosuspensions), small particles can be formed unintentionally during dissolution processes, e.g. upon dissolving larger-sized particles or due to precipitation of supersaturating drug delivery systems. The relative importance of the effects of absorbance by particulate matter can be expected to increase when having (i) lower solubilities of the compound in the dissolution medium, (ii) higher concentrations of solids, and (iii) smaller particle sizes. As Mie theory calculations proved successful in modeling the effect of particle size and suspension concentration on the resultant spectra, one can apply this approach as a first evaluation to determine the impact of particle absorption effects on solution concentration determinations for a given system.

ACKNOWLEDGMENTS

The authors would like to thank the National Science Foundation Engineering Research Center for Structured Organic Particulate Systems for financial support (NSF ERC-SOPS) (EEC-0540855). The authors thank the National Science Foundation, Directorate for Mathematical & Physical Sciences, Division of Materials Research for financial support (NSF MPS-DMR) (DMR-0804609). BVE is a Postdoctoral Researcher of the Fonds voor Wetenschappelijk Onderzoek, Flanders, Belgium. Prof. Dr. Ganesan Narsimhan and Dr. Xiaoyu Wu (Biochemical and Food Process Engineering, Department of Agricultural and Biological Engineering, Purdue University) are thanked for enabling the laser diffraction experiments. Dr. Huaping Mo (Purdue Interdepartmental NMR Facility, Department of Medicinal Chemistry and Molecular Pharmacology, Purdue University) is acknowledged for the NMR experiments. The authors would like to thank Prof. Dr. James D. Litster for use of the dynamic light scattering instrument. Pritesh Kerai is acknowledged for his assistance with the experiments.

REFERENCES

1. Berger CM, Tsinman O, Voloboy D, Lipp D, Stones S, Avdeef A. Technical note: miniaturized intrinsic dissolution rate (Mini-IDR (TM)) measurement of griseofulvin and carbamazepine. Dissolution Technol. 2007;14(4):39–41.
2. Avdeef A, Tsinman O. Miniaturized rotating disk intrinsic dissolution rate measurement: effects of buffer capacity in comparisons to traditional Wood's apparatus. Pharm Res. 2008;25(11):2613–27.
3. Tsinman K, Avdeef A, Tsinman O, Voloboy D. Powder dissolution method for estimating rotating disk intrinsic dissolution rates of low solubility drugs. Pharm Res. 2009;26(9):2093–100.
4. Avdeef A, Tsinman K, Tsinman O, Sun N, Voloboy D. Miniaturization of powder dissolution measurement and estimation of particle size. Chem Biodivers. 2009;6(11):1796–811.
5. Polster CS, Atassi F, Wu S, Sperry DC. Use of artificial stomach-duodenum model for investigation of dosing fluid effect on clinical trial variability. Mol Pharmaceutics. 2010;7(5):1533–8.
6. Josefson M, Johansson E, Torstensson A. Optical fiber spectrometry in turbid solutions by multivariate calibration applied to tablet dissolution testing. Anal Chem. 1988;60(24):2666–71.
7. Brown CW, Lin J. Interfacing a fiberoptic probe to a diode-array UV-visible spectrophotometer for drug dissolution tests. Appl Spectrosc. 1993;47(5):615–8.
8. Chen CS, Brown CW. A drug dissolution monitor employing multiple fiber optic probes and a UV/visible diode-array spectrophotometer. Pharm Res. 1994;11(7):979–83.
9. Cho J, Gemperline PJ, Walker D. Wavelength calibration method for a CCD detector and multichannel fiber-optic probes. Appl Spectrosc. 1995;49(12):1841–5.
10. Cho JH, Gemperline PJ, Salt A, Walker DS. UV-visible spectral dissolution monitoring by *in-situ* fiberoptic probes. Anal Chem. 1995;67(17):2858–63.
11. Aldridge PK, Melvin DW, Williams BA, Bratin K, Kostek LJ, Sekulic SS. A robotic dissolution system with online fiberoptic UV analysis. J Pharm Sci. 1995;84(8):909–14.
12. Aldridge PK, Kostek LJ. *In situ* fiber optic dissolution analysis. Dissolution Technol. 1995;2(4):10–1.
13. Rogers P, Hailey PA, Johnson GA, Dight VA, Read C, Shingler A, *et al.* A comprehensive and flexible approach to the automated-dissolution testing of pharmaceutical drug products incorporating direct UV-vis fiber-optic analysis, on-line fluorescence analysis, and off-line storage options. Lab Rob Auto. 2000;12(1):12–22.

14. Hengst R, Rolli R. Hollow shaft^{TM} sampling method in dissolution testing. Dissolution Technol. 1999;6(1):18–20.
15. Schatz C, Ulmschneider M, Altermatt R, Marrer S. Hollow shaft sampling with fiber optics. Dissolution Technol. 2000;7(1):20–1.
16. Schatz C, Ulmschneider M, Altermatt R, Marrer S, Altorfer H. Thoughts on fiber optics in dissolution testing. Dissolution Technol. 2001;8(2):1–5.
17. Bynum K, Roinestad K, Kassis A, Pocreva J, Gehrlein L, Cheng F, *et al.* Analytical performance of a fiber optic probe dissolution system. Dissolution Technol. 2001;8(4):1–8.
18. Johansson J, Cauchi M, Sundgren M. Multiple fiber-optic dual-beam UV/Vis system with application to dissolution testing. J Pharm Biomed Anal. 2002;29(3):469–76.
19. Lu X, Lozano R, Shah P. *In situ* dissolution testing using different UV fiber optic probes and instruments. Dissolution Technol. 2003;10(4):6–15.
20. Inman GW. Quantitative assessment of probe and spectrometer performance for a multi-channel CCD-based fiber optic testing system. Dissolution Technol. 2003;10(4):26–32.
21. Muhammad T, Wang J, Li-Wan M, Chen J. Monitoring dissolution rate of amiodarone tablets by a multiple fiber-optic sensor system. Dissolution Technol. 2008;15(1):22–7.
22. Martin CA. Evaluating the utility of fiber optic analysis for dissolution testing of drug products. Dissolution Technol. 2003;10 (4):37–40.
23. Toher CJ, Nielsen PE, Foreman AS, Avdeef A. *In situ* fiber optic dissolution monitoring of a vitamin B_{12} solid dosage formulation. 2003;10(4):20–5.
24. Gray VA. Dissolution testing using fiber optics—a regulatory perspective. Am Pharm Rev. 2003;6(2):26–30.
25. Gray VA. Dissolution testing using fiber optics—a regulatory perspective. Dissolution Technol. 2003;10(4):33–6 (reprint).
26. Mirza T, Liu Q, Vivilecchia R, Joshi Y. Comprehensive validation scheme for *in situ* fiber optics dissolution method for pharmaceutical drug product testing. J Pharm Sci. 2009;98 (3):1086–94.
27. Liu L, Fitzgerald G, Embry M, Cantu R, Pack B. Technical evaluation of a fiber-optic probe dissolution system. Dissolution Technol. 2008;15(1):10–20.
28. Wiberg KH, Hultin UK. Multivariate chemometric approach to fiber-optic dissolution testing. Anal Chem. 2006;78(14):5076–85.
29. Nie K, Li L, Li XX, Geng DS, Zhang QZ, Tuo MF, *et al. In situ* fiber-optic dissolution assisted by a mathematical separation model of dynamic three-wavelength K-ratio spectrophotometry. Dissolution Technol. 2010;17(2):15–8.
30. Van de Hulst HC. Light scattering by small particles. New York: Dover; 1981.
31. Bohren CF, Huffman DR. Absorption and Scattering of Light by Small Particles. New York: Wiley; 1983.
32. Alvarez MM, Khoury JT, Schaaff TG, Shafigullin MN, Vezmar I, Whetten RL. Optical absorption spectra of nanocrystal gold molecules. J Phys Chem B. 1997;101(19):3706–12.
33. Creighton JA, Eadon DG. Ultraviolet visible absorption-spectra of the colloidal metallic elements. J Chem Soc Faraday Trans. 1991;87(24):3881–91.
34. Jain PK, Lee KS, El-Sayed IH, El-Sayed MA. Calculated absorption and scattering properties of gold nanoparticles of different size, shape, and composition: applications in biological imaging and biomedicine. J Phys Chem B. 2006;110(14):7238–48.
35. Horn D, Rieger J. Organic nanoparticles in the aqueous phase—theory, experiment, and use. Chem Int Ed Engl. 2001;40 (23):4331–61.
36. Rabinow BE. Nanosuspensions in drug delivery. Nat Rev Drug Discovery. 2004;3(9):785–96.
37. Kesisoglou F, Panmai S, Wu Y. Nanosizing—Oral formulation development and biopharmaceutical evaluation. Adv Drug Deliv Rev. 2007;59(7):631–44.
38. Van Eerdenbrugh B, Van den Mooter G, Augustijns P. Top-down production of drug nanocrystals: Nanosuspension stabilization, miniaturization and transformation into solid products. Int J Pharm. 2008;364(1):64–75.
39. Brouwers J, Brewster ME, Augustijns P. Supersaturating drug delivery systems: the answer to solubility-limited oral bioavailability? J Pharm Sci. 2009;98(8):2549–72.
40. Lipinski C. Poor aqueous solubility—an industry wide problem in drug discovery. Am Pharm Rev. 2002;5(1):82–5.
41. Lindfors L, Forssen S, Skantze P, Skantze U, Zackrisson A, Olsson U. Amorphous drug nanosuspensions. 2. Experimental determination of bulk monomer concentrations. Langmuir. 2006;22 (3):911–6.
42. Savitzky A, Golay MJE. Smoothing and differentiation of data by simplified least squares procedures. Anal Chem. 1964;36(8):1627–39.
43. Van Eerdenbrugh B, Baird JA, Taylor LS. Crystallization tendency of active pharmaceutical ingredients following rapid solvent evaporation-classification and comparison with crystallization tendency from undercooled melts. J Pharm Sci. 2010;99 (9):3826–38.
44. Uesawa Y, Mohri K. Relationship between lipophilicities of 1, 4-dihydropyridine derivatives and pharmacokinetic interaction strengths with grapefruit juice. Yakugaku Zasshi. 2008;128 (1):117–22.
45. Fossheim R. Crystal structure of the dihydropyridine Ca^{2+} antagonist felodipine—dihydropyridine binding prerequisites assessed from crystallographic data. J Med Chem. 1986;29 (2):305–7.
46. Grant DJW, Brittain HG. Solubility of pharmaceutical solids. In: Brittain HG, editor. Physical characterization of pharmaceutical solids, drugs and the pharmaceutical sciences. New York: Marcel Dekker, Inc.; 1995. p. 321–86.
47. Van Eerdenbrugh B, Vermant J, Martens JA, Froyen L, Van Humbeeck J, Van den Mooter G, *et al.* Solubility increases associated with crystalline drug nanoparticles: methodologies and significance. Mol Pharmaceutics. 2010;7(5):1858–70.
48. Alonzo DE, Zhang GGZ, Zhou DL, Gao Y, Taylor LS. Understanding the behavior of amorphous pharmaceutical systems during dissolution. Pharm Res. 2010;27(4):608–18.
49. Lindfors L, Skantze P, Skantze U, Westergren J, Olsson U. Amorphous drug nanosuspensions. 3. Particle dissolution and crystal growth. Langmuir. 2007;23(19):9866–74.